

Coherent matter waves for ultrafast laser pulse characterization

M. Winter, M. Wollenhaupt, T. Baumert *

Experimentalphysik III, CINSaT, Institute of Physics, University of Kassel, Heinrich-Plett-Str. 40, D-34132 Kassel, Germany

Received 2 November 2005; accepted 23 December 2005

Abstract

A technique for the characterization of ultrashort laser pulses using coherent matter waves is demonstrated. We emphasize the analogy between matter wave packets and electromagnetic wave packets propagating in dispersive media. Due to quadratic dispersion the wave packets are stretched and their temporal structure eventually converges to their spectrum, thus providing a possibility for energy measurements in conjugate space. This is demonstrated theoretically and experimentally and is the basis for our laser pulse characterization technique. We use energy resolved interferometrically recorded photoelectron spectra generated by above-threshold ionization in an autocorrelation setup to characterize ultrashort laser pulses at 800 nm wavelength. This approach is potentially applicable to the XUV wavelength region.

© 2006 Elsevier B.V. All rights reserved.

1. Introduction

The characterization of ultrashort laser pulses is fundamental to their utilization in basic research and applications. Although a great variety of optical pulse characterization techniques is available in a spectral region ranging from infrared to ultraviolet the advent of attosecond pulses has necessitated to extend the spectral range of pulse characterization methods into the XUV region.

Generally the ultrashort duration of these pulses precludes a direct characterization of their temporal structure. However, in time domain information on the temporal structure of the pulse is extracted for example by non-linear autocorrelation techniques. Characterization methods operative in frequency domain—such as Spectral Interferometry (SI) [1]—or in the joint time/frequency domain—such as Frequency Resolved Optical Gating (FROG) [2]—complement the toolbox of the experimentalist. Recent measurements of the pulse spectrum in time domain [3] showed that the stringent distinction between techniques operative either in time domain or in frequency domain

is dispensable. In that work linearly chirped fiber gratings were used not only to stretch the pulse but also to convert the temporal pulse profile into the pulse's spectrum. This was achieved by introducing sufficient dispersion to temporally separate the spectral components. The interplay of dispersion and interference during coherent evolution of a system is a general principle which enables measurements of a physical quantity to be performed in its conjugate space.

We will exploit the coherent evolution of matter wave packets, i.e. structured free electron wave packets, in vacuum to demonstrate the measurement of the momentum distribution in coordinate space. Recently the interference of coherent matter waves has been demonstrated in weak [4,5] and strong laser fields [6] and interpreted in terms of a temporal Young's double slit experiment. In the present experiment we study the photoelectron spectra from multi-photon ionization of potassium atoms as a tool to characterize ultrashort laser pulses. To this end we will first demonstrate how the initial electron wave packet—determined by the properties of the ionizing laser pulse—evolves into its momentum distribution, i.e. the photoelectron spectrum. Because this process is quite analogous to the propagation of laser pulses in dispersive media used to measure pulse spectra in time domain, we point out the common physical

* Corresponding author. Tel.: +49 8153 281103; fax: +49 8153 281349.
E-mail address: tbaumert@physik.uni-kassel.de (T. Baumert).

principles in optics and quantum mechanics. An elucidating picture of physical effects caused by dispersion and interference connecting coordinate and momentum space is provided by the Wigner distribution in phase space.

We then discuss the above findings in terms of an application to laser pulse characterization. Measuring the Above Threshold Ionization (ATI) spectra introduces the required non-linearity to enable joint time/frequency characterization methods. In contrast to previous methods developed for ultrashort XUV pulses which either use second-order autocorrelation techniques [7] or energy resolved cross correlation techniques [8,9] we present a method using energy resolved photoelectron spectra recorded in an autocorrelation setup with interferometric resolution. In order to obtain information on the temporal structure of the pulse our measured energy resolved ATI spectra are converted into FROG traces. The temporal amplitude and phase of the pulse are retrieved using the principle components generalized projections algorithm [10,2] and compared to direct measurements in order to validate our technique. Because the presented procedure does not require optical elements to introduce non-linearities it is potentially applicable to the characterization of pulses in the XUV spectral region.

2. Interference of coherent matter waves

In this section we discuss the properties of coherent matter waves propagating in vacuum with respect to their optical analogue, i.e. the propagation of laser pulses in dispersive media. As an example we discuss the interference phenomena occurring during the propagation of a double peaked packet. The relation of the coordinate- and momentum space distribution is analyzed in phase space using the Wigner function.

2.1. Analogy to optics

We start by showing the analogy between the propagation of matter wave packets in vacuum—which is a dispersive medium for matter waves—and the propagation of light pulses in dispersive transparent media. The formal analogy is seen upon comparison of the ansatz for the time evolution of the wave function $w(x, t)$ in coordinate space and the temporal electrical field $E(x, t)$

$$w(x, t) \approx \frac{1}{2\pi} \int_{-\infty}^{\infty} w_0(k) e^{i[kx - \frac{\hbar k^2}{2m} t]} dk, \tag{1}$$

$$E(x, t) \approx \frac{1}{2\pi} \int_{-\infty}^{\infty} \tilde{E}_0(k) e^{i[kx - \frac{c^2 k^2}{2\omega^2} t]} dx, \tag{2}$$

where $w_0(k)$ describes the wave function in momentum space and $\tilde{E}_0(k)$ the spectrum of the pulse. The dispersion relation of free matter waves $\omega(k) \approx \frac{\hbar k^2}{2m}$ is responsible for the phase accumulated during the time evolution

$$\phi(k, t) \approx \frac{\hbar}{2m} k^2 t, \tag{3}$$

where m_e describes the electron mass, k the wave vector and t the propagation time. In contrast, material dispersion for electromagnetic waves originates from the frequency dependence of the refractive index $n(x)$. In order to emphasize the analogy to free matter waves we consider only the quadratic phase modulation of the transparent medium, which is by far the strongest contribution for most media of this type. Expressing the phase $\phi(x)$ in terms of the wave number $\phi(x) = k(x) \cdot x$, which is related to the refractive index $n(x)$ by $k(x) \approx \frac{n(x)\omega}{c}$, we obtain the cumulative phase for laser pulse propagation along the distance x by considering only the quadratic term of the Taylor series

$$\phi(x) \approx \frac{1}{2} \frac{\partial^2 \phi}{\partial x^2} x^2 \approx \frac{1}{2} \frac{\partial^2 k}{\partial x^2} x^2. \tag{4}$$

Substituting Eqs. (2) and (3) into Eq. (1) results in a representation that shows explicitly the complete analogy of the matter and the electromagnetic wave case within the limit of the approximation made

$$w(x, t) \approx \frac{1}{2\pi} \int_{-\infty}^{\infty} w_0(k) e^{i[kx - \frac{\hbar k^2}{2m} t]} dk, \tag{5}$$

$$E(x, t) \approx \frac{1}{2\pi} \int_{-\infty}^{\infty} \tilde{E}_0(k) e^{i[kx - \frac{c^2 k^2}{2\omega^2} t]} dx, \tag{6}$$

While the dispersion of matter waves parametrically depends on time, the dispersion of electromagnetic pulses parametrically depends on the propagation length. As a consequence of the quadratic phase factors in Eqs. (4) and (5) the initial distributions transform into their respective Fourier transforms. In optics, this was demonstrated by the measurement of the optical spectrum of an ultrashort laser pulse $\tilde{E}_0(k)$ in time domain [3]. In our contribution, we will focus on the measurement of the momentum distribution of matter waves $|w_0(k)|^2$ in coordinate space. In the experiment, matter waves are generated by photoionization and travel subsequently through a time-of-flight (TOF) electron spectrometer to be detected by a multichannel plate (MCP) as shown in the experimental setup in Fig. 2. Generally TOF data are interpreted in terms of momentum distributions of matter waves. However, the MCP detects the spatio-temporal distribution $|w(x, t)|^2$ of the electron wave packets. As the wave packet converges to the momentum distribution $|w_0(k)|^2$ for sufficiently long propagation in a medium characterized by quadratic dispersion, the momentum distribution is obtained by measuring the wave packet in coordinate space.

2.2. Interferences in phase space

In this section we discuss how the interplay of dispersion and interference converts the spatial distribution of a wave packet into its momentum distribution. We use the Wigner phase space representation of the wave packet [11] to visualize the time evolution in both coordinate and momentum space. The Wigner function is calculated based on the coordinate space representation of a wave function $w(x)$

$$W(\delta x, k) \approx \frac{1}{2\pi} \int_{-\infty}^{\infty} e^{ikn} w\left(x - \frac{1}{2}n\right) w\left(x + \frac{1}{2}n\right) dn, \quad (6)$$

or equivalently by starting with the momentum representation $\tilde{w}(k)$ [11]

$$W(\delta x, k) \approx \frac{1}{2\pi} \int_{-\infty}^{\infty} e^{ijx} \tilde{w}\left(k - \frac{1}{2}j\right) \tilde{w}\left(k + \frac{1}{2}j\right) dj. \quad (7)$$

The latter is more convenient in our case, because the time evolution of the momentum distribution of a wave packet is characterized by a simple phase factor as seen below in Eq. (10). The marginals of the Wigner function relate to the measured quantities, i.e. yield the momentum distribution

$$j \int_{-\infty}^{\infty} W(\delta x, k) dx \quad (8)$$

and the spatial distribution of the wave packet [11]

$$j \int_{-\infty}^{\infty} W(\delta x, k) dk \quad (9)$$

In our experiment we study the time evolution of a double peaked electron wave packet generated by multi-photon ionization of potassium atoms using a sequence of two ultrashort laser pulses as shown in Fig. 1a. Similar to the use of double pulse sequences in an optical autocorrelation setup we probe the coherence properties via coherent double peaked matter wave packets in a matter wave interferometer reminiscent of a temporal Young’s double slit experiment. The time evolution of the momentum distribution of such a free electron wave packet is given by

$$\tilde{w}(k) \approx \tilde{w}_0(k) e^{i\frac{\hbar k^2 t}{2m}} \left(1 \pm e^{i\frac{\hbar k_s^2 t}{2m}}\right), \quad (10)$$

$$\tilde{w}_0(k) \approx e^{i\frac{\hbar k_0^2 t}{2m}}, \quad (11)$$

where $\tilde{w}_0(k)$ describes the momentum distribution of the initial Gaussian wave packet. We calculate the Wigner function for this double peaked wave packet using Eq. (7) to obtain

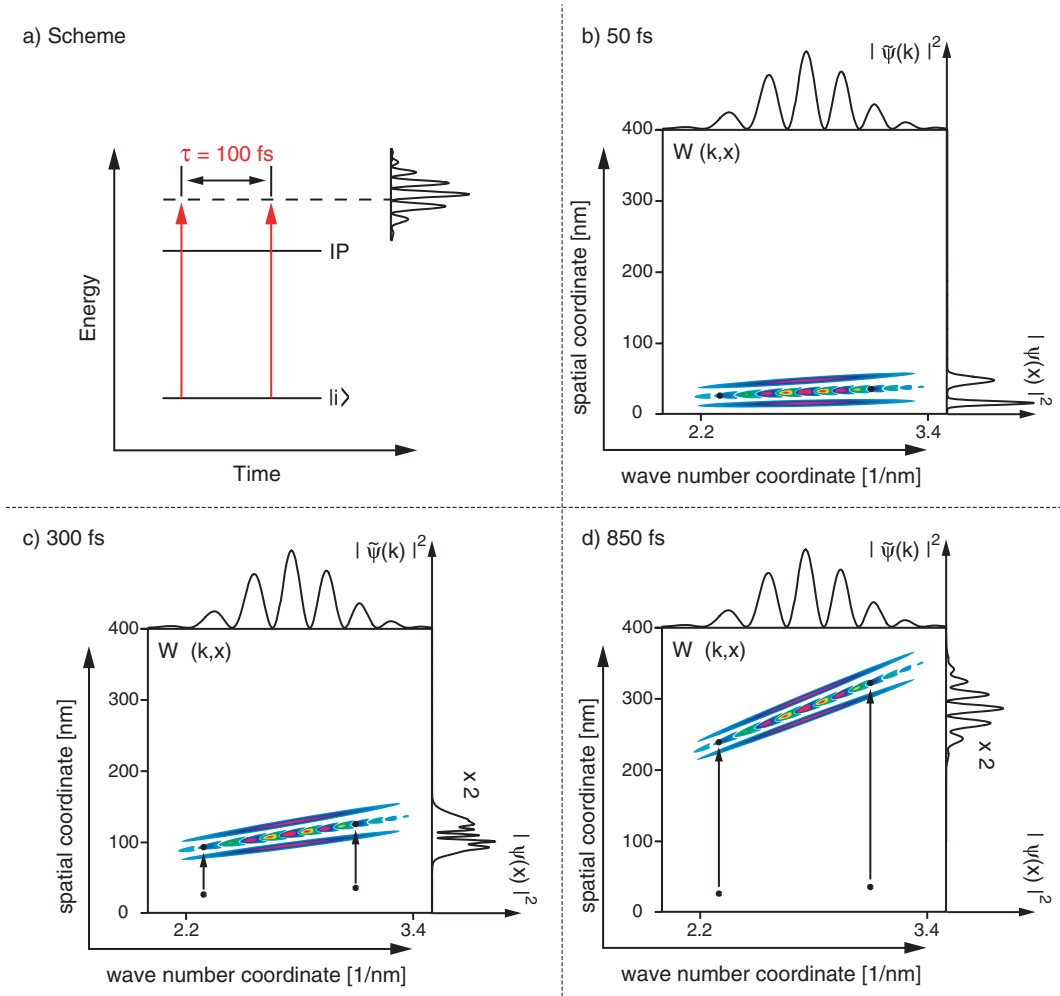


Fig. 1. (a) Ionization scheme, (b–d) snapshots of the Wigner function of a double peaked matter wave packet created 0.3 eV above the ionization potential at propagation times of 50, 300 and 850 fs. On top of the phase space plot the momentum distribution $j \int W(\delta x, k) dx$ is shown. To the right the spatial distribution $j \int W(\delta x, k) dk$ is depicted. Both distributions are marginals of the Wigner function. The increasing tilt of the Wigner function at later propagation times results in the appearance of fringes in the spatial distribution. In addition the trajectories of classical particles are indicated by the black dots and arrows in the phase space plots.

$$W_1(x, k) = \frac{1}{4} \int_{-\infty}^{\infty} \int_{-\infty}^{\infty} p dk e^{-\frac{\hbar k_0 p^2}{4c}} \left[e^{-X^2 T^2 \delta t^2} p e^{-X^2 T^2 \delta t^2} \left(\frac{C_1}{2} \right) \cos \left(\frac{1}{2} \left[\arctan \left(\frac{C_1}{2} \right) \right] \right) \right. \\ \left. - \frac{C_2^2}{c^2} \int_{-\infty}^{\infty} \int_{-\infty}^{\infty} \frac{C_1 X T \delta t^2 \delta C_2}{c} X T \delta t^2 \right] \quad (12)$$

where k describes wave number coordinate which is a measure of the momentum $\hbar k$ and x the spatial coordinate and using the abbreviations $\delta k = \frac{\hbar k_0}{2}$, $X = \frac{\hbar}{2m} dk$, $C_1 = \frac{X^2 x_{sm}}{\hbar}$, $C_2 = kxXs$ and $T \delta t^2 = \frac{\delta m x}{\hbar k} \delta t^2$. The envelope of the momentum distribution is governed by the leading exponential function, reminiscent of the shape of the exciting laser pulses. The next two terms describe the temporal evolution of the single wave packets. The last summand describes the cross term of both wave packets [11]. The oscillatory structure of the cross term is accounted for by the cosine term while the envelope is described by the exponential part.

As an example, we show the time evolution of a double peaked electron wave packet created by a laser pulse sequence separated by a time delay of $s = 100$ fs with a kinetic energy of approximately 0.3 eV. In Fig. 1b–d snapshots of the Wigner function are shown at increasing propagation times. In addition, the corresponding marginals, i.e. the coordinate representation of the wave packet $|w(x)|^2$ and its the momentum distribution $|w(k)|^2$ are displayed. For comparison we illustrate the trajectories of classical particles with low and high momentum in Fig. 1c and d.

In the phase space plots the Wigner functions of the individual wave packets are of elliptical shape due to their Gaussian profile. In between the two ellipses we observe the aforementioned characteristic interference- or cross terms which take positive and negative values [11]. At $t = 0$ fs the cross terms cancel out upon integration along the momentum coordinate, reproducing the double peaked structure in coordinate space.

In Fig. 1b a snapshot of the Wigner function of the wave packet at $t = 50$ fs is depicted. In phase space, propagation in a dispersive medium leads to a slight tilt of the Wigner function. In coordinate space this tilt corresponds to a broadening of the wave packet. At $t = 50$ fs the broadening is seen by comparison of the leading and the trailing wave packet. Classically the motion of the wave packet can be understood in terms of the different propagation velocities of classical particles since the high momentum particles travel faster than the low momentum particles. This provides a classical picture of the tilt in the contour of the Wigner function as the wave packet propagates through the medium. At later propagation times the tilt increases such that the cross-terms no longer cancel out in coordinate space. Fig. 1c shows the Wigner function at an intermediate time $t = 300$ fs. At this time transient interferences are observed in coordinate space, indicating that both wave packets merge into one another. In Fig. 1d at $t = 850$ fs the tilt results in a Wigner function which is nearly symmetrical

with respect to the coordinate- and the momentum axis. This provides an illustrative explanation how the spatial distribution of the wave packet $|w(x)|^2$ eventually converges to the momentum distribution $|w(k)|^2$.

The experimental scheme to study the coherence properties of free electron wave packets is shown in Fig. 2. The setup has already been briefly described in [4] and will be described here in more detail. A 1 kHz Ti:sapphire laser system providing 1 mJ, 30 fs ultrashort laser pulses at a central wavelength of 790 nm is used. The laser beam at the fundamental wavelength is first split into two beams, one of which is frequency doubled to provide 0.25 IJ, 405 nm photons with perpendicular polarization. The other beam is delayed by 4 ns and then coupled into a Mach-Zehnder interferometer to generate a pair of two identical laser pulses (1 IJ, $<10^{12}$ W/cm², 30 fs at 790 nm) with a well defined temporal spacing s . All three beams are then recombined and focussed into a high vacuum chamber where a beam of atomic potassium K(4s) intersects perpendicularly with the femtosecond laser pulses leading to photoionization. The frequency doubled beam is used to prepare the K atoms in the (5p) state as the initial state in our experiment. Light at the fundamental wavelength ionizes the K(5p) atoms in a one photon process. The energy spectrum of the released threshold photoelectrons is then detected by a magnetic bottle-type time-of-flight (TOF) electron spectrometer with an energy resolution of 25 meV for electrons with a kinetic energy of 1 eV. Additionally the spectrum of the laser pulse sequence is detected in order to independently check the time delay via the separation of the interference fringes. The laser energy is monitored continuously by a photodiode. In order to ensure interferometric accuracy of the translation stage creating the femtosecond pulse sequence, the interference signal from a HeNe laser beam after passing through a Mach-Zehnder interferometer attached to the translation stage is measured.

Because the time-of-flight within the magnetic bottle spectrometer is in the order of a few hundred nanoseconds, i.e. much longer than the time interval in which the transient interferences are observed, the detected spatial distribution is quasi stationary. As a consequence, the spatial distribution has converged to the momentum distribution as depicted in Fig. 1d. This enables us to measure the momentum distribution of free electron wave packets in coordinate space.

In the case of a double peaked wave packet in space the corresponding momentum distribution consists of a characteristic interference pattern as discussed in [4]. In that work it was shown that the photoelectron spectrum is related to the power spectral density (PSD) of the laser pulses by

$$P_e(x_e) \propto \int_{-\infty}^{\infty} \cos(\delta x_{ph} s) PSD(\delta x_{ph}) ds \quad (13)$$

with $\hbar x_e = \frac{\hbar}{2m} \delta x_{ph} \delta x_{IP}$, where $\hbar x_{5p}$ denotes the excitation energy of the K(5p) state, $\hbar x_{IP}$ the ionization potential and $\hbar x_{ph}$ the photon energy of the driving electric

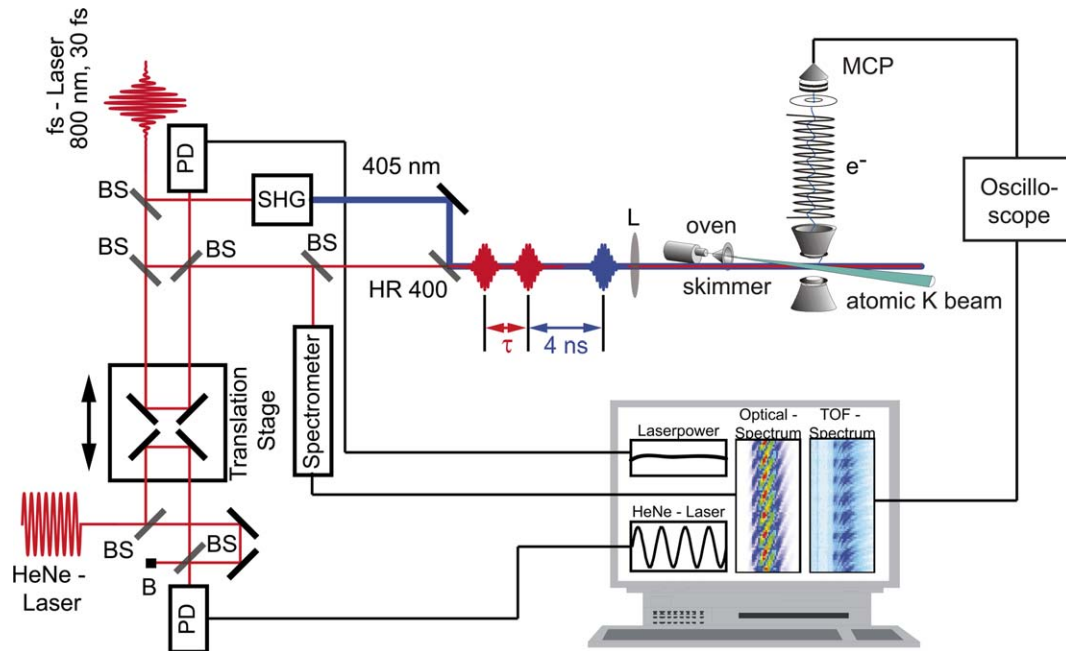


Fig. 2. The experimental scheme to characterize ultrashort laser pulses and measure matter wave interferences. A fs laser beam is split up into three parts of which one is frequency doubled to prepare the K(5p) state as initial state of the experiments. The fundamental pulses are delayed by 4 ns to this pulse and can be delayed to one another by the Mach-Zehnder setup. Additional mirrors for adjusting the delays are not shown in this scheme. Laser power and optical spectrum are measured in parallel. For comparison with the characterization experiments a second-order autocorrelation was measured using a lens and a two-photon diode just before the focussing lens. The HeNe Mach-Zehnder setup which is also mounted to the translation stage is used to ensure interferometric accuracy. (BS = beamsplitter, B = blocker, SHG = Second Harmonic Generator, HR400 = dichroic mirror highly reflective at 400 nm, PD = photodiode, L = focussing lens ($f = 30$ cm), MCP = multichannel plate).

field. An example of the spectrum produced by a double peaked wave packet generated by two laser pulses delayed by 240 fs is shown in Fig. 3. The photoelectron spectrum shows the expected interference fringes [4] resulting from the tilt in Wigner space with an energy spacing of $\frac{h}{s} \approx 17$ meV. The low modulation of the interference fringes is due to the low energy separation of the fringes being at the limit of the energy resolution of our TOF spectrometer.

3. Pulse characterization

In this section we extend the above findings to nonlinear ionization as a tool to characterize ultrashort laser pulses using matter waves. Multi-photon ionization of atoms is used as non-linear medium rather than optical frequency conversion techniques. Therefore our approach is potentially applicable to the XUV spectral region. In order to verify the validity of our pulse characterization approach, we apply our method to 800 nm laser pulses for which other established characterization techniques are available. This procedure enables us to compare the results obtained via photoelectron spectroscopy with independently measured optical techniques such as second-order autocorrelations.

So far we have considered a linear ionization process. However, for the temporal characterization of an ultrashort laser pulse nonlinear processes are required due to Wiener's theorem, which states that the Fourier transform

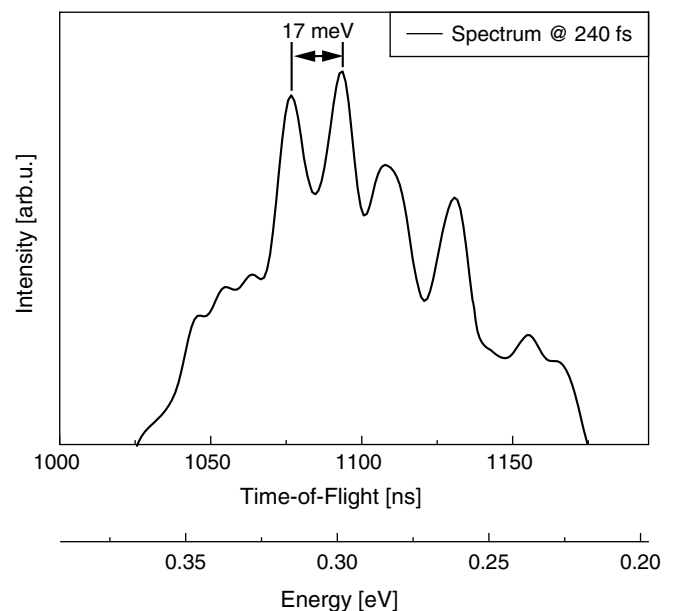


Fig. 3. Time-of-flight signal of electron wave packets generated by a $s = 240$ fs separated fs laser pulse pair. The laser pulses serve as temporal slits in the time-energy domain [4] analogous to Young's double-slit experiment, thus leading to spectral interferences. The fringes due to the laser pulse sequence are clearly visible. Since the propagation time in the magnetic-bottle spectrometer is sufficiently long the time distribution can be converted to an energy distribution. The fringe spacing is $\frac{h}{s} \approx 17$ meV.

of a first-order (linear) autocorrelation function is the PSD of the corresponding function. Therefore the linear autocorrelation function is not sensitive to spectral phase modulation. Consequently we extend the discussion to nonlinear ionization processes using above-threshold ionization (ATI). In our pulse characterization scheme we analyze energy resolved two-photon ATI photoelectron spectra from an interferometric pulse sequence. The laser pulse energy in this experiment is kept rather low. The ratio of the first to the second ATI was about 10 to 1. In this regime the influence of higher ATI on the measurement is neglected. Conventional SHG-FROG traces are recovered from the interferometric measurement by Fourier filtering [12]. In our experiment we employ a collinear setup depicted in Fig. 2. The ATI electrons are measured to introduce the required non-linearity into the measurement process. In order to obtain an interferometric signal the delay between the 2 fs laser pulses of fundamental wavelength has been varied from 0 fs to 100 fs in 0.12 fs steps. The spacing of the interference fringes decreases with increasing delay between the pulses. At 100 fs the spacing corresponds to 40 meV and is in the range of the resolution of our spectrometer. This is on the same order as the resolution of our TOF electron spectrometer at 1.9 eV. Lowering the resolution in simulations by a factor of two did not change the accuracy of the retrieved pulse shape within the error limits. For every time step an ATI photoelectron spectrum consisting of an average over 3000 laser shots has been recorded. For comparison with our characterization results with the help of the ATI spectra a second-order autocorrelation has been measured independently in front of the focussing lens. Similar to the threshold measure-

ments the K(5p) state is prepared to be the initial state of the measurement. Starting from this state ionization by two photons of the fundamental wavelength gives rise to ATI. Because this non-resonant process is analogous to optical second harmonic generation, we apply the filtering process introduced in [12] to our data, as described below.

In order to convert the recorded interferometric ATI photoelectron spectra (shown in Fig. 4c) into a valid SHG-FROG trace we analyze the data within a range of time delays from 0 fs to 100 fs. The measured spectra are mirrored around time zero to provide a complete interferometric ATI-FROG trace. This complete signal is first Fourier transformed along the delay axis. The resulting trace is shown in Fig. 4d in which the different frequency components at $x = 0$, $x = x_0$ and $x = 2x_0$ with $x_0 = 2.66 \text{ fs}^{-1}$ are clearly distinguished from one another. For comparison a simulated trace (taking into account an unchirped 30 fs Gaussian laser pulse) is shown in Fig. 4b. The energy integrated signal of the simulated and measured traces—which yield the respective second-order autocorrelation functions—are shown in Fig. 4a. Good agreement of both curves confirms the validity of our approach. The residual difference is due to deviations of the actual pulse shape in comparison to the simple pulse shape assumed in the simulation.

After filtering out the x_0 and $2x_0$ components and inverse Fourier transform into time domain, the residual weak background is subtracted. Finally the photoelectron energy axis is calibrated with respect to angular frequencies of the exciting laser pulses. This results in a valid SHG-FROG trace which is then retrieved using the principal components general projections retrieval algorithm intro-

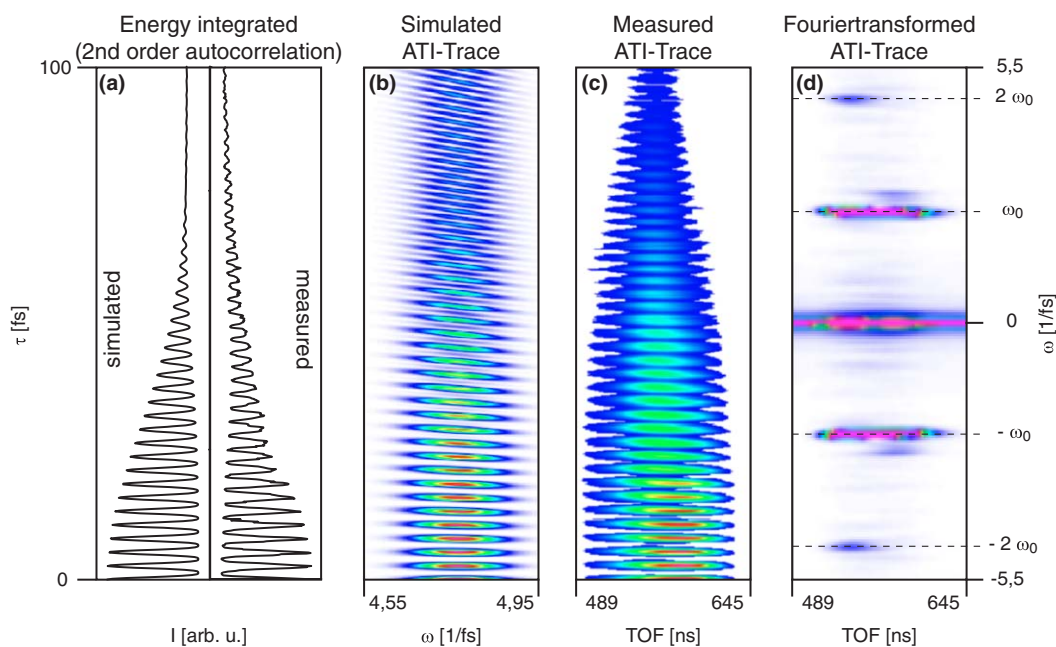


Fig. 4. (a) Comparison of the energy integrated signals of (b) and (c). (b) Simulated interference ATI trace employing 30 fs, 800 nm gaussian laser pulses. (c) Measured interference ATI trace. (d) Fourier transform of (c) along the delay axis. The different frequency components are clearly distinguished.

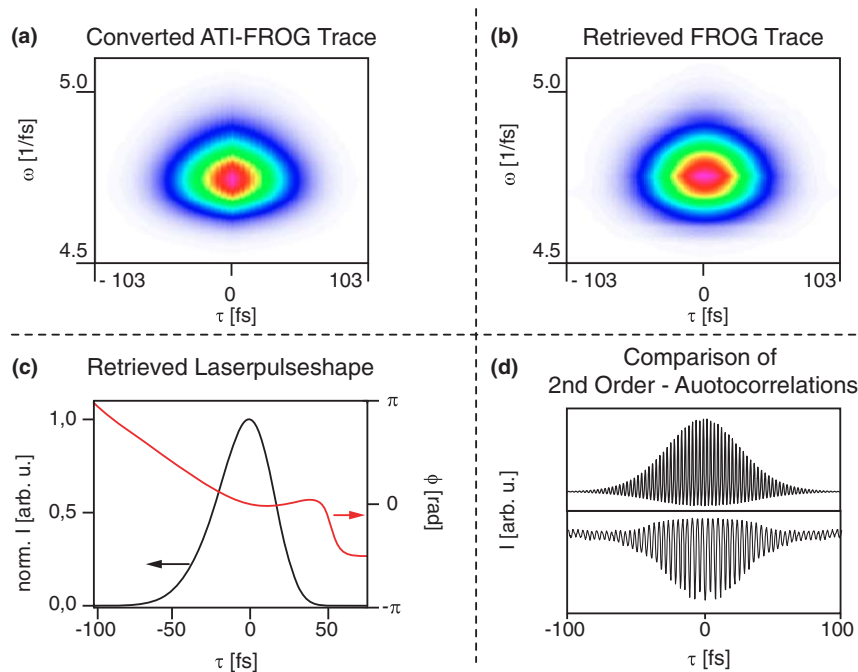


Fig. 5. (a) SHG-FROG trace prepared from the interferometric ATI trace. (b) Retrieved SHG-FROG trace. The rms difference to (a) is 0.6%. (c) Retrieved pulse intensity and phase. The pulse duration is 42 fs (FWHM) with a linear Chirp of 326 fs^2 . (d) Comparison of the directly measured second-order autocorrelation function (bottom) and the second-order autocorrelation function calculated from the retrieved pulse (top).

duced by Kane [10]. The SHG-FROG trace obtained in this way is shown in Fig. 5a. In Fig. 5b the retrieved trace is depicted. The FROG error, i.e. the rms of the difference between the measured and retrieved trace, is 0.6% [2]. The corresponding pulse shape is displayed in Fig. 5c. A pulse duration of $42 \pm 3 \text{ fs}$ (FWHM) is measured. The phase function exhibits a linear chirp of 326 fs^2 . This value is in accordance with the linear chirp introduced by the focusing lens and the dichroitic beamsplitter used to recombine the frequency doubled laser pulse with the fundamental pulse pair. A comparison of the second-order autocorrelation calculated from the retrieved pulse shape and the independently measured second-order autocorrelation is presented in Fig. 4d. The autocorrelation was measured in front of the focussing lens (see Fig. 2) using a two-photon photodiode. Good agreement between both traces confirms the accuracy of our method.

4. Conclusion

We demonstrated the use of coherent matter waves for characterization of ultrashort laser pulses. The analogy between light propagation in dispersive media and the propagation of free coherent matter waves in vacuum was used to illustrate measurements of a physical quantity in conjugate space. The underlying physical mechanism based on the interplay of dispersion and interference was depicted in Wigner phase space. After sufficiently long coherent time evolution the Wigner distribution was symmetrical with respect to coordinate and momentum space

indicative to the convergence of the wave packet into its momentum distribution. As an example we showed how an initially double peaked free electron wave packet subjected to dispersion converges to its momentum distribution characterized by interference fringes. Experimentally, the double peaked wave packet was generated by a sequence of two ultrashort laser pulses and measured by threshold photoelectron spectroscopy. The resulting interference pattern in the photoelectron spectrum is reminiscent of a Young's double-slit experiment with matter waves performed in time. By using a time-of-flight spectrometer the momentum distribution was measured in coordinate space. This technique was then applied to characterize fs laser pulses. The required non-linearity was introduced by using the first ATI peak of the photoelectron spectrum to avoid resonances which could potentially distort the FROG trace due to their lifetime. The spectrally resolved interferometric ATI signal was converted to a SHG-FROG trace to which a standard SHG-FROG retrieval algorithm was applied. This yielded the temporal structure of the fs laser pulses used in the experiment. Exemplifying our strategy we employed 800 nm femtosecond laser pulses to compare the results with independently measured second-order autocorrelation functions. The comparison shows good agreement confirming the validity of our approach.

As the technique only requires a non-linear (non-resonant) ionization process the extension to the XUV spectral region is straightforward. Within that context the detection of above-threshold ionization in rare gases using 25 eV

photons has been demonstrated [13]. In addition constant ionization probability within the entire bandwidth of the broadband attosecond ionization has to be assured and the temporal response of the process needs to be faster than the pulses to be characterized [14].

Acknowledgements

We like to thank D. Liese and O. Gräfe for technical assistance on the molecular beam apparatus and C. Sarpe-Tudoran for operating the femtosecond laser system. We gratefully acknowledge the financial support by the Deutsche Forschungsgemeinschaft.

References

- [1] L. Lepetit, G. Chériaux, M. Jore, J. Opt. Soc. Am. B 12 (1995) 2467.
- [2] R. Trebino, Frequency-Resolved Optical Gating, Kluwer Academic Publishers, Norwell, 2002.
- [3] J. Azaña, L.R. Chen, M.A. Muriel, P.W.E. Smith, Electron. Lett. 35 (1999) 2223.
- [4] M. Wollenhaupt, A. Assion, D. Liese, C. Sarpe-Tudoran, T. Baumert, S. Zamith, M.A. Bouchene, B. Girard, A. Flettner, U. Weichmann, G. Gerber, Phys. Rev. Lett. 89 (2002) 173001-1.
- [5] F. Lindner, M.G. Schätzel, H. Walther, A. Baltuška, E. Goulielmakis, F. Krausz, D.B. Milošević, D. Bauer, W. Becker, G.G. Paulus, Phys. Rev. Lett. 95 (2005) 040401-1.
- [6] M. Wollenhaupt, A. Präkelt, C. Sarpe-Tudoran, D. Liese, T. Baumert, J. Opt. B 7 (2005) S270.
- [7] P. Tzallas, D. Charalambidis, N.A. Papadogiannis, K. Witte, G.D. Tsakiris, Nature 426 (2003) 267; P. Tzallas, D. Charalambidis, N.A. Papadogiannis, K. Witte, G.D. Tsakiris, J. Mod. Opt. 52 (2005) 321.
- [8] R. López-Martens, J. Mauritsson, A. Johansson, J. Norin, A. L'Huillier, Eur. Phys. J. D 26 (2003) 105.
- [9] T. Sekikawa, T. Katsura, S. Miura, S. Watanabe, Phys. Rev. Lett. 88 (2002) 193902-1; T. Sekikawa, T. Kanai, S. Watanabe, Phys. Rev. Lett. 91 (2003) 103902-1.
- [10] D.J. Kane, IEEE Quant. Electr. 35 (1999) 421.
- [11] L. Cohen, Time-Frequency Analysis, Prentice Hall, Upper Saddle River, 1995; S. Qian, D. Chen, Joint Time-Frequency Analysis: Methods and Applications, Prentice Hall, Upper Saddle River, 1996; W.P. Schleich, Quantum Optics in Phase Space, Wiley, VCH, Berlin, 2001.
- [12] I. Amat-Roldán, I.G. Cormack, P. Loza-Alvarez, Emilio J. Gualda, D. Artigas, Opt. Expr. 12 (2004) 1169.
- [13] N. Miyamoto, M. Kamei, D. Yoshitomi, T. Kanai, T. Sekikawa, T. Nakajima, S. Watanabe, Phys. Rev. Lett. 93 (2004) 083903-1.
- [14] L.A.A. Nikolopoulos, E.P. Benis, P. Tzallas, D. Charalambidis, K. Witte, G.D. Tsakiris, Phys. Rev. Lett. 94 (2005) 113905-1.

Available online at www.sciencedirect.com

Optics Communications 281 (2008) 895

 OPTICS
COMMUNICATIONS

www.elsevier.com/locate/optcom

Erratum

Erratum to: “Coherent matter waves for ultrafast laser pulse characterization” [Opt. Commun. 264 (2006) 285]

M. Winter, M. Wollenhaupt, T. Baumert *

Experimentalphysik III, CINSaT, Institute of Physics, University of Kassel, Heinrich-Plett-Str. 40, D-34132 Kassel, Germany

Received 28 September 2007; accepted 4 October 2007

The abbreviation c in the Wigner function of two interfering free electron wave packets in Eq. (12) on p. 288 was not defined. The correct definition of c is given by

$c = \frac{1}{4} \sqrt{\frac{Dk^4 s^2 \hbar^2}{16m^2}}$. An additional amendment is related to the value of x_0 in line 16 on p. 290 (right column). The correct value for x_0 is 2.36 fs⁻¹.

 DOI of original article: [10.1016/j.optcom.2005.12.079](https://doi.org/10.1016/j.optcom.2005.12.079).

* Corresponding author. Tel.: +49 561 804 4452; fax: +49 561 804 4453.

E-mail address: tbaumert@physik.uni-kassel.de (T. Baumert).